The 2014 World Congress on
Advances in Civil, Environmental, and Materials Research (ACEM14)
Busan, Korea, August 24-28, 2014

Three dimensional structural and aeroelastic effects on long-span bridges with respect to flutter critical states

*Ting-ting Ma[1)] and Yao-jun Ge[2)]

[1), 2)] *State Key Laboratory of Disaster Reduction in Civil Engineering, Tongji University, Shanghai, China*
[*] *tingtinghorse@126.com*

ABSTRACT

Three-dimensional (3D) effects with respect to 3D structural response and 3D aeroelastic forces on critical flutter wind speed are investigated via numerical and experimental methods. Two-dimensional (2D) flutter analysis towards 2D bridge section and full-order flutter analysis for 3D structure are both carried out on two cable-supported bridges 2D aeroelastic forces, the effect of 3D aeroelastic forces on flutter wind speed is and an imaginary simply-supported beam bridge, based on which, the 3D structural effect is discussed for bridges with different main spans and different deck sections. Furthermore, wind tunnel tests with a full aeroelastic model are performed for the simply-supported beam bridge. With the comparison with the analytical results using the 3D structure and traditional concluded.

1. INTRODUCTION

Aeroelastic study with regards to flutter phenomenon is a fundamental part of long span bridge design in order to ensure their stability. The aeroelastic behavior of bridges under wind loads can be predicted by wind tunnel tests or analytical approaches with two dimensional (2D) and three dimensional (3D) models. However, whether for experimental or analytical methods, there are uncertain differences in flutter prediction between 2D and 3D results. Factors leading to the deviation of the critical flutter states between 2D bridge section and 3D full structure can be divided into four major categories: multimode response effect (i.e., 3D structural effects), aerodynamic interference effects of cables on deck, aeroelastic effects of cables and 3D aeroelastic effects (i.e., spatial correlation effects of flutter derivatives, the end effects or the influence of variant additional static wind angle of attack on aeroelastic forces)).

The problem of multimode response of long-span bridges to wind excitations and the effect upon incrementing the number of modes participating in flutter analysis have been depicted in several investigations (e.g., Tanaka et al. 1993; Miyata et al. 1994; Jain et al. 1996; Katsuchi et al. 1999; Ge & Tanaka 2000), and the higher modes present an uncertain effect, which may lead to a reduction or increase of critical flutter

---

[1)] Graduate Student
[2)] Professor

wind speed. The aerodynamic interference effects of cables were considered by Katsuchi (1999) towards the Akashi Kaikyo Bridge. Two different sets of flutter derivatives, measured using sectional models with different main cable heights, were applied to the 340 m long section at the center where main cables are close to the deck and influence deck stability aerodynamically. However, no comparative study was conducted in this research to identify the aerodynamic interference effects of cables. Another investigation conducted by Yang (2012) presented an obvious increase in flutter speed with the consideration of the local vibrations and aerodynamic forces of the stay cables. The 3D aeroelastic effects on flutter was first investigated by Scanlan (1997) with the introduction of a new parameter to take into account the potential loss in correlation of the flutter derivatives along the deck of the bridge, and was subsequently used by Katsuchi (1999) as one of the probable factors responsible for the difference between 3D analytical and wind tunnel test results of the Akashi Kaikyo Bridge. However, the influence of other potential factors, such as aerodynamic forces on cables, was not effectively separated.

The focus of this paper is, first, to carry out further studies on the 3D structural effects towards bridges with different main spans and different deck sections and, second, to investigate the 3D aeroelastic effects. An iterative flutter analysis with 2D bridge section and the full-order flutter analysis with 3D bridge model were both carried out on two cable-stayed bridges with the spans of 605m and 1088m and one simply-supported beam bridge with a span of 300m, based on which, the 3D structural effect is discussed and summarized. The 3D aeroelastic effects on flutter wind speed with regard to the simple beam bridge were separated by means of a well-designed wind tunnel test with a full aeroelastic model.

2. FLUTTER ANALYSIS

2.1 2D flutter analysis

A bridge deck section is assumed to have two degrees-of-freedom: bending displacement h and torsional displacement α. The equation of motion is:

$$\begin{cases} m(\ddot{h} + 2\xi_h \omega_h \dot{h} + \omega_h^2 h) = L \\ I_m(\ddot{a} + 2\xi_\alpha \omega_\alpha \dot{a} + \omega_\alpha^2 a) = M \end{cases} \quad (1)$$

where m and I_m represent the mass and mass moment of inertia per unit length of the deck section, respectively; ω_h and ω_α are the circular frequencies for the heaving and pitching mode, respectively, and ξ_h and ξ_α are the corresponding modal damping ratios. Forces L and M represent the aerodynamic lift and moment about the rotation axis per unit span. The expressions for L and M for a bluff deck section were proposed by Scanlan (1971):

$$\begin{cases} L = \rho U^2 B\left[KH_1^*(K)\dfrac{\dot{h}}{U} + KH_2^*(K)\dfrac{B\dot{a}}{U} + K^2 H_3^*(K)a + K^2 H_4^*(K)\dfrac{h}{B}\right] \\ M = \rho U^2 B^2\left[KA_1^*(K)\dfrac{\dot{h}}{U} + KA_2^*(K)\dfrac{B\dot{a}}{U} + K^2 A_3^*(K)a + K^2 A_4^*(K)\dfrac{h}{B}\right] \end{cases} \tag{2}$$

where ρ is the air density, U is the uniform approach velocity of wind and B is the deck width. In these equations, the coefficients $H_i^*(K)$ and $A_i^*(K)$ (i =1, 2, 3, 4) are considered to be experimentally determined functions of K, where $K=B\omega/U$, ω being the oscillation circular frequency. Inserting Eq. 2 into Eq. 1 and rewriting it in the matrix form yields

$$M\ddot{q} + C\dot{q} + Kq = 0 \tag{3}$$

The coefficient matrices in Eq. 3 are defined as follows:

$$M = \begin{bmatrix} m & 0 \\ 0 & I_\alpha \end{bmatrix},\ q = \begin{bmatrix} h \\ \alpha \end{bmatrix} = \begin{bmatrix} h_0 \\ \alpha_0 \end{bmatrix} e^{st}$$

$$C = \begin{bmatrix} 2m\xi_h\omega_h - \rho UBKH_1^* & -\rho UB^2 KH_2^* \\ -\rho UB^2 KA_1^* & 2I_\alpha\xi_\alpha\omega_\alpha - \rho UB^3 KA_2^* \end{bmatrix}$$

$$K = \begin{bmatrix} m\omega_h^2 - \rho U^2 K^2 H_4^* & -\rho U^2 BK^2 H_3^* \\ -\rho U^2 BK^2 A_4^* & I_\alpha\omega_\alpha^2 - \rho U^2 B^2 K^2 A_3^* \end{bmatrix}$$

Since the equation of motion of flutter, Eq. 3, has the frequency dependent components, the solution for the critical flutter wind speed has to be done in an iterative way. The procedure in present paper for determination of critical flutter wind speed is presented in Fig. 1.

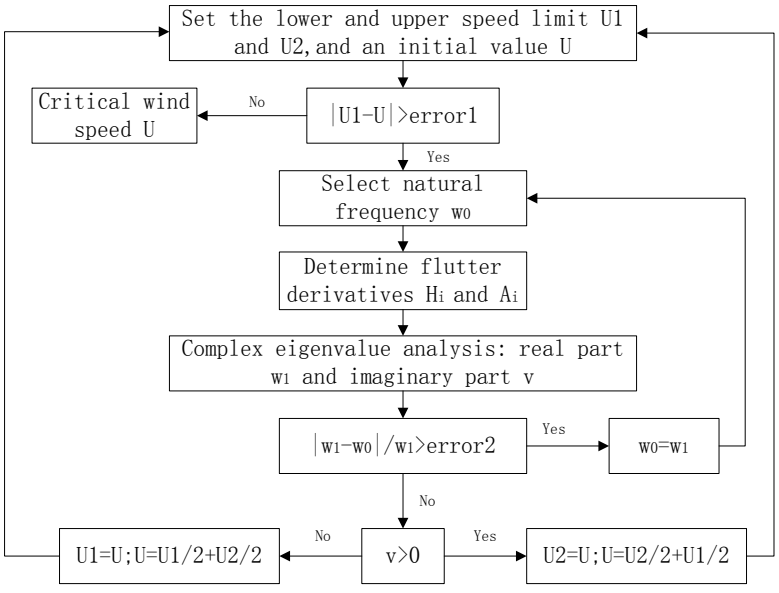

Fig. 1 Procedure for 2D flutter analysis

2.2 3D Full-order flutter analysis

The equation of motion for a bridge with *n*-DOFs in the smooth flow can be expressed as

$$M_s\ddot{X} + C_s\dot{X} + K_s X = F_{se} \tag{4}$$

where M_s, C_s and K_s are the global mass, damping and stiffness matrices, respectively; X , $\dot{X}$ and $\ddot{X}$ represent the nodal displacement, velocity and acceleration vectors, respectively; and F_{se} denotes the vector of nodal aeroelastic forces.

The motion-dependent aeroelastic forces distributed on unit span of bridge girder are expressed as a linear function of nodal displacement and nodal velocity

$$\begin{cases} L = \rho U^2 B\left[KH_1^*\dfrac{\dot{h}}{U} + KH_2^*\dfrac{B\dot{a}}{U} + K^2H_3^*a + K^2H_4^*\dfrac{h}{B} + KH_5^*\dfrac{\dot{p}}{U} + K^2H_6^*\dfrac{p}{B}\right] \\ D = \rho U^2 B\left[KP_1^*\dfrac{\dot{p}}{U} + KP_2^*\dfrac{B\dot{a}}{U} + K^2P_3^*a + K^2P_4^*\dfrac{p}{B} + KP_5^*\dfrac{\dot{h}}{U} + K^2P_6^*\dfrac{h}{B}\right] \\ M = \rho U^2 B^2\left[KA_1^*\dfrac{\dot{h}}{U} + KA_2^*\dfrac{B\dot{a}}{U} + K^2A_3^*a + K^2A_4^*\dfrac{h}{B} + KA_5^*\dfrac{\dot{p}}{U} + K^2A_6^*\dfrac{p}{B}\right] \end{cases} \tag{5}$$

In these equations, $H_i^*(K)$, $P_i^*(K)$ and $A_i^*(K)$ (i =1, 2, 3, 4, 5, 6) are functions of the reduced frequency K. The self-excited forces are applied to the FE model in the form of elemental aeroelastic stiffness and damping matrices, which can be realized in ANSYS by using Matrix27 element type. By converting the distributed aeroelastic forces of element *e* of bridge girder into equivalent nodal loadings at member ends, the stiffness and damping matrices applied to one of the member ends, contributed by element *e*, can be expressed as

$$K_{M27} = a\begin{bmatrix} 0 & 0 & 0 & 0 & 0 & 0 \\ 0 & -H_4^* & H_6^* & BH_3^* & 0 & 0 \\ 0 & P_6^* & -P_4^* & -BP_3^* & 0 & 0 \\ 0 & BA_4^* & -BA_6^* & -B^2A_3^* & 0 & 0 \\ 0 & 0 & 0 & 0 & 0 & 0 \\ 0 & 0 & 0 & 0 & 0 & 0 \end{bmatrix},\ a = \rho U^2K^2L_e/2 \tag{6a}$$

$$C_{M27} = b\begin{bmatrix} 0 & 0 & 0 & 0 & 0 & 0 \\ 0 & -H_1^* & H_5^* & BH_2^* & 0 & 0 \\ 0 & P_5^* & -P_1^* & -BP_2^* & 0 & 0 \\ 0 & BA_1^* & -BA_5^* & -B^2A_2^* & 0 & 0 \\ 0 & 0 & 0 & 0 & 0 & 0 \\ 0 & 0 & 0 & 0 & 0 & 0 \end{bmatrix},\ b = \rho UBKL_e/2 \tag{6b}$$

where L_e denotes the length of element e. The sign of each item in K_{M27} and C_{M27} is closely related to the definition of the coordinate direction both for the aeroelastic forces and the FE model.

The full-order flutter analysis procedure is performed in the physical coordinate. The contribution of all modes to flutter can be taken into account. The computation of critical flutter wind speed needs a sweep-and-iteration procedure based on complex eigenvalue analyses and mode trace. A more comprehensive explanation of this methodology can be found in the work developed by Hua (2007), whose computational code programmed in ANSYS has been used to obtain the flutter wind speed.

3. 3D STRUCTURAL RESPONSE EFFECT

Based on the 2D and 3D flutter analyses methods, as was mentioned above, the effect of 3D structural response on critical flutter state was investigated towards Sutong Bridge, Qingzhouminjiang Bridge and a pseudo simply-supported beam bridge. The deviation of 3D flutter analysis results from 2D values is attributed to the 3D structural response effects (more exactly, the contribution of the higher modes).

3.1 Description of the target bridges

3.1.1 Sutong Bridge

The Sutong Bridge (Fig. 2) is a 7-span cable-stayed bridge over the Yangtse River in China with the longest main span among cable-stayed bridges. The main span is 1088 m and there are six symmetric side spans of 100 m, 100 m, and 300 m. The Bridge consists of two inverse Y-shaped concrete towers, double-plane fan type cables and a streamlined steel box girder bridge deck. The width of the deck is 41 m. There are in total 272 (34×8) stay cables.

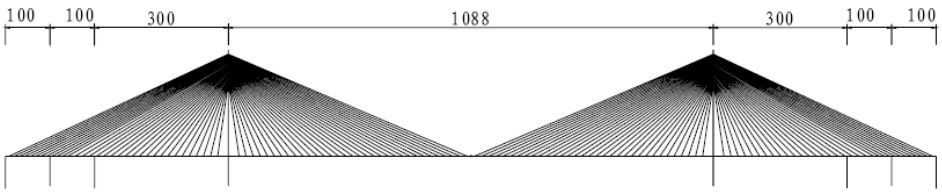

Fig. 2 General layout of the Sutong Bridge (Units: m)

3.1.2 Qingzhouminjiang Bridge

The Qingzhouminjiang Bridge (Fig. 3) is a cable-stayed bridge in China with a main span of 605m, which ranks the first among the completed composite-deck cable-stayed bridges. The composite-deck system of the bridge has an open-section consisting of two main I-shaped steel girders, steel floor beams and 25 cm thickness concrete slab. The steel girders are 2.45 m high and 27 m separated from each other. The width of the deck is 29 m. The two towers are diamond-shaped concrete structures. There are in total 21×8=168 stay cables with the longest cable being over 312 m.

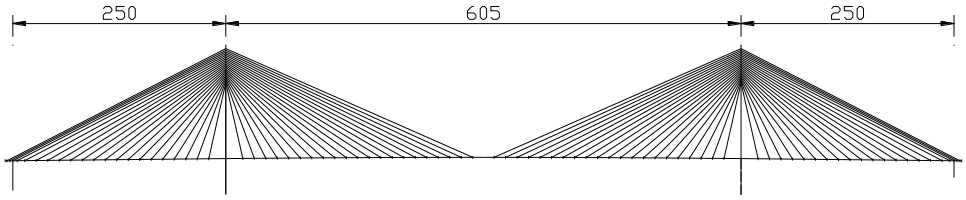

Fig. 3 General layout of the Qingzhouminjiang Bridge (Units: m)

3.1.3 Simply-supported beam bridge

The simply-supported beam bridge (Fig. 4) with a span of 300 m is an imaginary structure designed mainly for the full aeroelastic wind tunnel tests, which will be described in more detail below. The suspenders illustrated in Fig. 4, with no mass, were specially designed to satisfy the requirements for small displacements and relatively low flutter wind speed (Ucr<100 m/s). The main parameters of the simple beam bridge are as follows: the vertical moment of inertia I_{zz}=1.8 m^4; the lateral moment of inertia I_{yy}=95 m^4; the free torsional moment of inertia I_{xx}=1.64 m^4; mass m=20000 kg/m; mass moment of inertia I_m=1800000 kg·m^2/m; the elastic stiffness of the suspenders k=924400 kg/m. The naked steel box of the Runyang Suspension Bridge in China, with deck width of 36.3 m, was selected for the simple beam bridge deck.

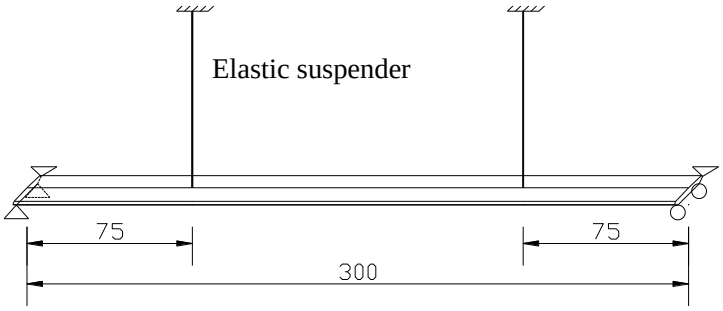

Fig. 4 Schematic diagram of the pseudo simply-supported bridge (Units: m)

3.2 Dynamic properties of the target bridges

Modal analysis based on FE models is the first important step towards flutter prediction. The FE models of the target bridges have been developed in ANSYS with a simple single-girder beam element deck model. The frequencies of several important modes are listed in Table 1. Corresponding equivalent mass m_{eq} and equivalent mass moment of inertia I_{eq} calculated by

$$m_{i_s eq} = \frac{\int m\varphi^2 dx}{\int_{L_{girder}} \varphi_{bi_s}^2(x)\,dx}, \quad I_{i_s eq} = \frac{\int m\varphi^2 dx}{\int_{L_{girder}} \varphi_{ti_s}^2(x)\,dx} \tag{7}$$

are also listed in Table 1. In these equations subscript *i* denotes the i^{th} mode, $\int m\varphi^2 dx$ represents the generalized mass of the i^{th} mode, L_{girder} represents the integration along the bridge deck, subscript *s* (*s*=*x*, *y*, *z*, *rotx*) denotes the component in s-direction, and subscripts *b* and *t* represent the bending and torsional modes, respectively.

Table1 Modal properties of the target bridges

Mode shape	Sutong Bridge		Qingzhouminjiang Bridge		Simply supported bridge	
	Frequency (Hz)	m_{eq} (or I_m)	Frequency (Hz)	m_{eq} (or I_m)	Frequency (Hz)	m_{eq} (or I_m)
1-S-L	0.1142	26946.5	0.2183	31471	0.5538	20014
1-S-V	0.1891	29913.3	0.2045	35251	0.2614	20017
1-S-T	0.5166	4740720	0.4670	2295770	0.4521	1801250
1-AS-L	0.3194	27864.7	0.6349	43990	2.206	20055
1-AS-V	0.2314	30142.9	0.2478	37076	0.4914	20055
1-AS-T	0.7808	4219610	0.5510	3270300	0.9038	1804960

Note: S and AS represent symmetric and asymmetric, respectively; L, V and T denote the lateral, vertical and torsional mode, respectively; the unit of m_{eq} is kg/m; the unit of I_m is kg·m^2/m

3.3 Aeroelastic forces of the target bridges

Two sets of aerodynamic derivatives, identified through the wind tunnel tests with sectional models of a typical box section and a Π-shaped section (Fig. 5), respectively, are both employed to simulate the aeroelastic forces applied to the three target bridges. The dimension of the cross sections in Fig. 5 corresponds to the sectional models in wind tunnel tests. The dimension of deck width B for flutter analysis is 30.25 m for steel box section and 29 m for Π-shaped open section. The flutter derivatives at 0° angle of attack are illustrated in Fig. 6.

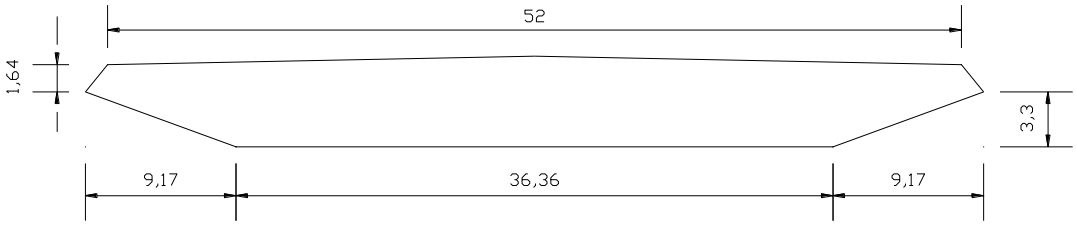

(a) Steel box section

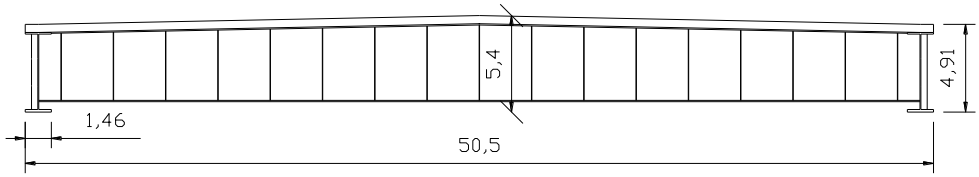

(b) Π-shaped section

Fig. 5 Two sets of typical deck sections (Units: cm)

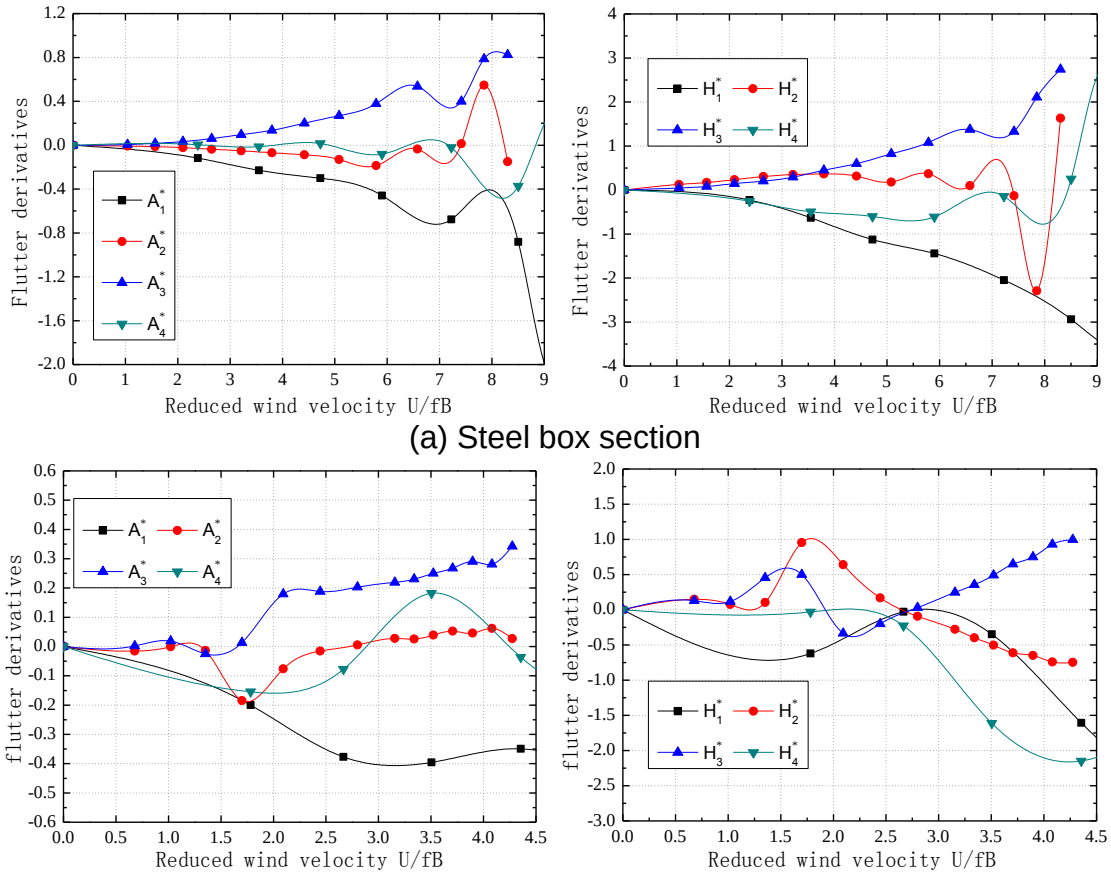

(a) Steel box section

(b) Π-shaped section

Fig. 6 Flutter derivatives of the typical deck sections

3.4 3D Structural effects on flutter

Two-dimensional flutter analysis with the full-scaled sectional model and full-order flutter analysis with the 3D structure are carried out towards the three target bridges mentioned above. The modal parameters for 2D flutter analyses are taken from Table 1 with respect to the first vertical bending and torsional modes, which have been verified to be the most important modes in 3D flutter analysis. The modal damping ratios are set to be zero. The calculated critical flutter wind speeds corresponding to the steel box section and Π-shaped section are listed in Table 2.

Table 2 Critical flutter wind speed (Units: m/s)

Target bridge	Sutong Bridge		Qingzhouminjiang Bridge		Simply-supported beam bridge	
Deck section	Π-shaped	Box	Π-shaped	Box	Π-shaped	Box
U_{cr} (2D)	39.5	97.3	35.1	83.8	33.8	77.4
U_{cr} (3D)	34.2	94.4	35.4	82.7	34.1	77.4
Deviations	-13.4%	-3.0%	0.9%	-1.3%	0.9%	0%

Analysis results in Table 2 indicate that the contribution of the higher modes to flutter wind speed could be positive or negative, as presented in the research

achievements of previous studies. Moreover, the 3D structural response effect is generally more significant corresponding to the longer main-span bridges. The configuration of the deck section may play an important role in the 3D structural response effect on flutter speed, particularly for super-long-span bridges. Based on the examples presented, conclusions may be expanded that the higher mode effects can be neglected for bridges with main-span of hundreds of meters. But for super-long-span bridges, sectional model tests may result in great deviation in flutter prediction because of the insufficiently reflected 3D structural effects.

4. 3D AEROELASTIC EFFECT

Three-dimensional flutter analyses using a 3D structure and traditional 2D aeroelastic forces obtained from sectional model tests neglect the potential influence of span-wise correlation of the flutter derivatives, the end effects and the influence of additional static wind angle of attack (changing along the bridge) on aeroelastic forces, which are defined as 3D aeroelastic effects in present paper. The 3D aeroelastic effects were investigated via wind tunnel tests with a full aeroelastic model scaled from the pseudo simply-supported beam bridge mentioned above. For its simplicity in structure, the full aeroelastic model can effectively exclude the aerodynamic interference effects of cables and aerodynamic forces acting on cables.

4.1 Design of the full aeroelastic model

The aeroelastic model was designed using the Froude similarity, adopting a geometrical scaling factor of 1:100. Fig. 7 shows the overall picture of the aeroelastic model during wind tunnel testing. The deck consists of an internal steel spine and an external covering made of modeling foam. The former is designed to represent the scaled elastic properties of the real structure, while the latter reproduces the external aerodynamic shape and it accounts for mass distribution. The external covering was divided into ten sections with a gap of 1-2 mm left between each other. The geometry of the cross section can be found in Fig. 8. The mass and the mass moment of inertia are tuned by the addition of lumped iron masses in each module of the external covering, in order to achieve the target values. A pair of springs hanging in the roof of the wind tunnel, connected to the deck by thin constantan wires, was adopted to reproduce the axial stiffness of the suspenders. Besides, the boundary conditions are the same with those shown in Fig. 4.

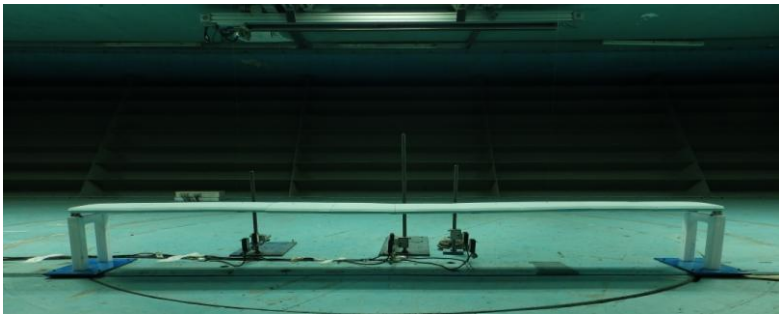

Fig. 7 Aeroelastic model in wind tunnel

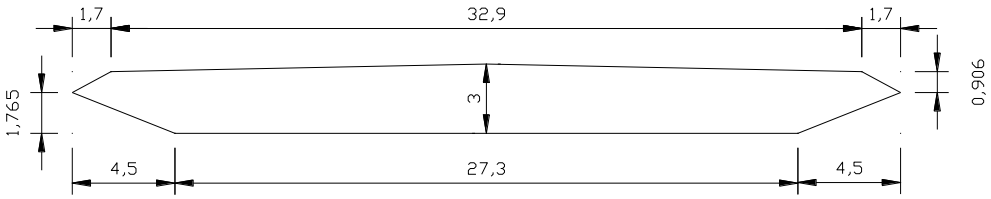

Fig. 8 Cross section of the aeroelastic model (Units: cm)

4.2 Verification of dynamic properties

It is important to keep the modal properties of the aeroelastic model the same with those obtained from FE model analysis, thus eliminating the influence of structural difference on flutter prediction. The main properties of the first vertical and torsional modes of the aeroelastic model, identified through a frequency analysis of the free motion response of the bridge, are summarized and compared with the FE model results in Table 3. Fig. 9 depicted the comparison between the identified experimental mode shapes and the numerical FE model results. Modal properties shown in Table 3 and Fig. 9 present much correspondence between the calculated and experimental measured results, which provides a precondition for subsequent comparison between experimental results and 3D flutter analysis results.

Table 3 Comparison of structural dynamic properties

Mode shape	Measured damping ratio	Measured f_m (Hz)	Calculated f_c (Hz)	$(f_m-f_c)/f_c$ (%)
1-S-V	0.005	2.610	2.614	-0.2
1-S-T	0.007	4.492	4.521	-0.6

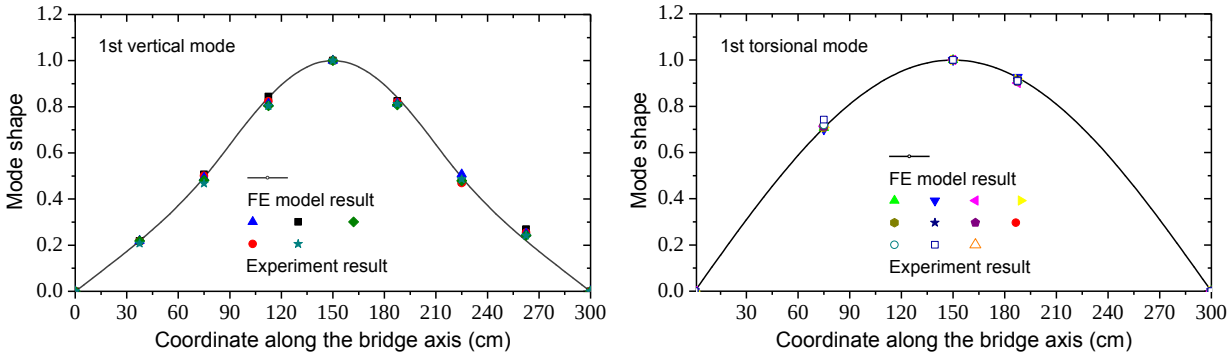

Fig. 9 Verification of mode shapes

It is noteworthy that, due to the manufacturing error, the structural parameters of the simple beam bridge in Section 3.1.3 with respect to the structural stiffness have been the result of a complex inverse derivation procedure based on the measured modal properties. Since only the first modes were measured, further verification needs to be conducted for the accuracy of the baseline FE model. In the experiments, the mass and the mass moment of inertia are tuned by changing the quantity and the distribution of

the lumped iron masses glued inside the external covering. The same adjustments were done towards the baseline FE model. Modal properties of the first modes are measured for each mass condition and compared with corresponding FE modal analysis results, as shown in Table 4. The fact that little deviation exists between computed and measured modal properties with regard to different structural mass condition further demonstrates the accuracy of the baseline FE model for the aeroelastic model.

Table 4 Comparison of structural dynamic properties

m (kg/m)	I_m (kg·m²/m)	1-S-V			1-S-T		
		f_m (Hz)	f_c (Hz)	$(f_m-f_c)/f_c$ (%)	f_m (Hz)	f_c (Hz)	$(f_m-f_c)/f_c$ (%)
2	0.018	2.610	2.614	-0.2	4.492	4.521	-0.6
2	0.016	2.610	2.614	-0.2	4.776	4.761	0.3
2.204	0.018	2.504	2.490	0.6	4.545	4.521	0.5
1.796	0.018	2.752	2.758	-0.2	4.545	4.521	0.5

4.3 Wind tunnel tests

The wind tunnel tests with the full aeroelastic model were carried out in the TJ-3 Boundary Layer Wind Tunnel (overall size of 14 m length, 15 m width and 2 m height) in Tongji University, under the smooth flow condition. The different mass conditions of the aeroelastic model, as shown in Table 4, are considered in the experiments. The determination of the critical flutter state is according to the obviously observed divergence phenomenon. The measurement precision for flutter wind speed is less than 0.1 m/s. The critical flutter wind speeds U_{cr} as well as the flutter frequencies f_{cr} measured from wind tunnel tests are shown in Table 5.

4.4 3D Full-order flutter analyses

In order to compare with the experimental results, the 3D full-order flutter analyses were performed towards the aeroelastic model based on the 2D aeroelastic forces. The flutter derivatives are identified through a numerical forced vibration method with the amplitude of vibration of 2 degrees. A detailed description of the forced vibration method can be found in literatures (Liu & Ge 2013; Ge & Liu 2014). The Reynolds number during the identification procedure was 2×10^5. It is almost the same with the value corresponding to the critical flutter state (Re = UD/v = $8.5\times0.363/0.000015$ = 2.057×10^5) in wind tunnel tests, which can effectively eliminating the potential Reynolds number effect on aerodynamic forces. Fig. 10 shows the identified aerodynamic derivatives of the naked steel box section (Fig. 8).

The modal damping properties are simulated as the Rayleigh damping based on the damping ratios of first vertical mode and the first torsional mode. According to the measured damping ratios in wind tunnel tests (Table 3), the values of 0.005 and 0.007 are set as the damping ratios of first vertical mode and the first torsional mode, respectively. 3D flutter analysis results of different mass conditions are listed in Table 5 and compared with the experimental results

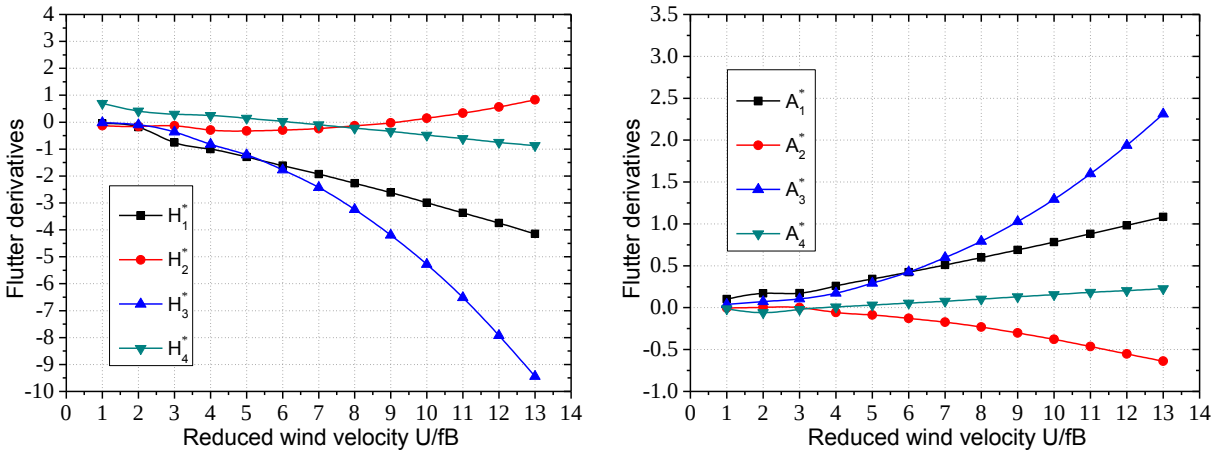

Fig. 10 Flutter derivatives of the steel box deck of the aeroelastic model

Table 5 Summary of the flutter characteristics of the aeroelastic model

m (kg/m)	I_m (kg·m²/m)	Analytical results (A)		Experimental results (E)		(E/A-1)×100	
		U_{cr} (m/s)	f_{cr} (Hz)	U_{cr} (m/s)	f_{cr} (Hz)	U_{cr}	f_{cr}
2	0.018	8.850	3.566	8.49	3.693	-4.07	3.56
2	0.016	9.242	3.640	8.94	3.729	-3.27	2.45
2.204	0.018	9.197	3.438	8.94	3.551	-2.79	3.29
1.796	0.018	8.441	3.699	8.31	3.729	-1.55	0.81

4.5 Discussions on the 3D aeroelastic effect

Because of the almost identical structural parameters between the aeroelastic model and corresponding baseline FE model and the effectively elimination of Reynolds effect on aerodynamic forces, the differences between analytical results and experimental results in Table 5 can be probably attributed to the effects of 3D aerodynamic forces. However, before the conclusion is reached, the potential influence of another factor with respect to the damping characteristics of the high modes needs to be investigated. As was mentioned above, the first vertical and torsional modal damping ratios for 3D flutter analysis were equal to those measured in wind tunnel tests, while the damping ratios for higher modes were simulated by Rayleigh damping, as shown in Fig. 11. On the other hand, the damping ratios of the higher modes have not been identified in wind tunnel tests, i.e. the deviation of higher-mode-related damping ratios between analytical and experimental models was unknown. Direct contrast analysis is therefore unavailable. Thus, a two-step sensitivity analysis procedure towards the higher-mode-related damping ratios was carried out.

The first step focuses on the investigation of the higher-mode contribution to flutter wind speed, which can be realized through the comparison between 2D and 3D flutter

analysis results shown in Table 6. Results indicate a negligible participation of the higher modes in flutter phenomenon. The contrast study between 2D and 3D flutter analysis with modal damping ratios being zero, as shown in Table 6, was additionally conducted as the second step. The almost equal small differences between 2D and 3D analysis results with respect to different structural damping demonstrates that the higher modes and the higher-mode-related damping ratios have little influence on the critical flutter wind speed in the example presented.

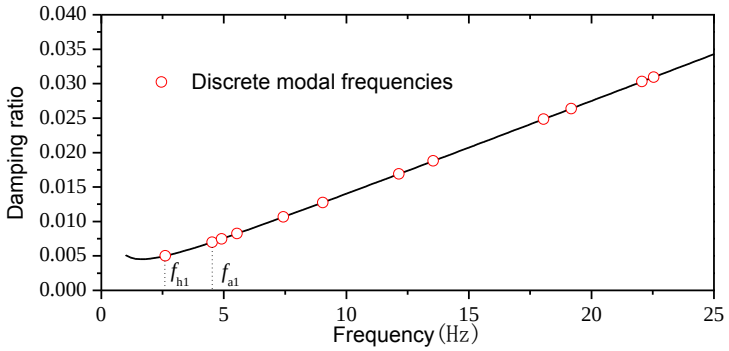

Fig. 11 Modal damping ratios for FE model

Table 6 Analytical flutter characteristics of the aeroelastic model

ξ_h	ξ_α	2D results		3D results		(3D-2D)/2D	
		U_{cr} (m/s)	f_{cr} (Hz)	U_{cr} (m/s)	f_{cr} (Hz)	U_{cr} (%)	f_{cr} (%)
0.005	0.007	8.774	3.584	8.850	3.566	0.87	-0.50
0	0	8.485	3.646	8.561	3.626	0.90	-0.55

Based on the detailed discussions above, a conclusion can be reached that the 3D aeroelastic effects result in a drop of critical flutter wind speed by 1.55%~4.07% in the present 300 m-main-span simple beam bridge.

5. CONCLUSIONS

Three dimensional structural and aeroelastic effects on flutter critical states were investigated through analytical and experimental methods. The iterative flutter analysis with 2D bridge section and the full-order flutter analysis with 3D bridge FE model were both carried out on two cable-stayed bridges with the spans of 605m and 1088m and one pseudo simply-supported beam bridge with a span of 300m based on the same aerodynamic forces corresponding to a typical Π-shaped deck section and a streamlined box deck section, and the computational flutter critical speeds have the relative differences of +0.9% and 0%, respectively, in the 300m span, +0.90% and -1.3% in 605m, and -13.4% and -3.0% in 1088m. The contribution of the higher modes to flutter wind speed could be positive or negative. Moreover, the 3D structural response effects become more significant with the increase of span length. The configuration of the deck section may play an important role in the 3D structural

response effect on flutter speed, particularly for super-long-span bridges.

Experimental investigation was conducted in the TJ-3 Boundary Layer Wind Tunnel with a full aeroelastic model of the simple beam bridge. Different structural mass conditions were considered and a maximum decrease of 4.07% in flutter critical speed was observed compared with the 3D full-order flutter analysis results, which is considered to be the effect of 3D aeroelastic forces.

ACKNOWLEDGEMENTS

The work described in this paper is partially supported by the NSFC under the Grant 91215302 and by the MOST under the 973 Program Grant 2013CB036301.

REFERENCES

Ge, Y.J. and Liu, S.Y. (2014), "2D Pure-numerical simulation for whole-process wind-induced responses of long-span bridge decks", *The 6th International Symposium on Computational Wind Engineering*, Hamburg, Germany.

Ge, Y.J. and Tanaka, H. (2000), "Aerodynamic flutter analysis of cable-supported bridges by multi-mode and full-mode approaches", *J. Wind Engrg. Industr. Aerodyn.*, 86,123-153.

Hua, X.G., Chen, Z.Q., Ni, Y.Q. and Ko, J.M. (2007), "Flutter analysis of long-span bridges using ANSYS", *Wind Struct.*, 10(1), 61-82.

Jain, A., Jones, N.P. and Scanlan, R.H. (1996), "Coupled flutter and buffeting analysis of long-span bridges", *J. Struct. Engrg.*, 122, 716-725.

Katsuchi, H, Jones, N.P. and Scanlan, R.H. (1999), "Multimode coupled flutter and buffeting analysis of the Akashi-Kaikyo Bridge", *J. Struct. Engrg.*, 125, 60-70.

Liu, S.Y. and Ge, Y.J. (2013), "Fitting Method of Nonlinear Differential Equations for Aerodynamic Forces of Bridge Decks", *The 12th Americas Conference on Wind Engineering*, Seattle, USA.

Miyata, T., Tada, K., Sato, H., Katsuchi, H. and Hikami, Y. (1994), "New findings of coupled-flutter in full model wind tunnel tests on Akashi Kaikyo Bridge", *Proc., Symp. on Cable-stayed and Suspension Bridges*, Association Francaise Pour la Construction, Deauville, France, 163-170.

Scanlan, R. H., Jones, N. P., & Lorendeaux, O. (1997). "Comparison of taut-strip and section-model-based approaches in long-span bridge aerodynamics", *J. Wind Engrg. Industr. Aerodyn.*, 72, 275-287.

Scanlan, R.H. and Tomko, J.J. (1971), "Airfoil and bridge deck flutter derivatives", *J. of Engrg. Mech.*, ASCE, 97(6):1717-1737.

Tanaka, H., Yamamura, N. and Shiraishi, N. (1993), "Multi-mode analysis and two & three dimensional model tests on bridges with non-analogous modal shapes", *J. Struct. Mech. and Earthquake Engrg*., Tokyo, Japan 10(2), 35-46.

Yang, D.C., Ge, Y.J. and Xiang, H.F. (2012), "Influences of local vibrations of cables on flutter behaviors of cable-stayed bridges", *The Seventh International Colloquium on Bluff Body Aerodynamics and Applications (BBAA7)*, Shanghai, China, September 2-6, 2012.